Polarization dependence of laser damage growth features on multilayer dielectric mirrors for petawatt-class lasers

Saaxewer Diop, Marine Chorel, Alexandre Ollé, Nadja Roquin, Éric Lavastre, Laurent Gallais, Nicolas Bonod, Laurent Lamaignère

Polarization dependence of laser damage growth features on multilayer dielectric mirrors for petawatt-class lasers

SAAXEWER DIOP[1,2,*], MARINE CHOREL[1], ALEXANDRE OLLÉ[1,2], NADJA ROQUIN[1], ÉRIC LAVASTRE[1], LAURENT GALLAIS[2], NICOLAS BONOD[2], AND LAURENT LAMAIGNÈRE[1]

[1] *Commissariat à l'Énergie Atomique et aux Énergies Alternatives - Centre d'Études Scientifiques et Techniques d'Aquitaine (CEA-CESTA), F-33116 Le Barp, France*
[2] *Aix-Marseille Univ, CNRS, Centrale Marseille, Institut Fresnel, 13013 Marseille, France*
[*] *Corresponding author: saaxewer.diop@cea.fr*

Compiled November 1, 2022

PETAL (PETawatt Aquitaine Laser) is an ultra-high-power laser dedicated to academic research that delivers sub-picosecond pulses. One of the major issues on these facilities is the laser damage on optical components located at the final stage. Transport mirrors of the PETAL facility are illuminated under different polarization directions. This configuration motivates thorough investigation of the dependency of the laser damage growth features (thresholds, dynamics and damage site morphologies) with the incident polarization. Damage growth experiments were carried out in *s* and *p*-polarization at 0.8 ps and 1053 nm on multilayer dielectric mirrors with a squared top-hat beam. Damage growth coefficients are determined by measuring the evolution of the damaged area for both polarizations. In this paper, we report higher damage growth threshold in *p*-polarization together with higher damage initiation threshold in *s*-polarization. We also report faster damage growth dynamics in *p*-polarization. The damage site morphologies and their evolution under successive pulses are found to strongly depend on polarization. A numerical model in 3D was developed to assess this experimental observations, it shows the relative differences in damage growth threshold however, it was not able to reproduce the damage growth rate. Numerical results demonstrate that damage growth is mainly driven by the electric field distribution which depends on the polarization.

http://dx.doi.org/10.1364/ao.XX.XXXXXX

As the energy of high-power laser facilities is limited by laser-induced damage on optical components located after the amplification stage, the understanding of laser damage mechanisms has become a major issue [1]. In the sub-picosecond regime, laser damage initiation follows a deterministic behavior which is directly linked to the Electric Field Intensity (EFI) [2]. Optical components of petawatt-class lasers are generally composed of Multilayer Dielectric (MLD) coatings which provide high intrinsic damage threshold [3]. The reflections of the incident laser on the multiple interfaces provide interferences which could enhance the EFI distribution in the components and decrease the effective damage threshold [4, 5].

The beam of the PETAL (PETawatt Aquitaine Laser) facility [6], is linearly polarized after the compression stage. Depending on their position in the transport section, mirrors are illuminated either in *s* or in *p*-polarization. The EFI and the Laser Induced Damage Threshold (LIDT) are both dependent on polarization [7]. The electric field enhancement is lower in *s*-polarization which leads to a higher LIDT in the sub-picosecond and picosecond regimes [8]. After the occurrence of a damage site, the damage area evolves with successive laser shots which ultimately limits the lifetime of the optics [9].

Several studies evidenced a deterministic behavior of the damage growth features by measuring the growth threshold at a fluence under the LIDT. Above the growth threshold, a linear evolution of the damaged area was reported in Ref. [10]. Sozet *et al.* measured a polarization dependence on MLD mirrors with a growth threshold in *s*-polarization which represents approximately 50% of $LIDT_s$ (LIDT in *s*-polarization) [11]. A growth threshold in *p*-polarization representing 80% of $LIDT_p$ (LIDT in *p*-polarization) was reported with a very slow evolution of the damaged area. A study of the polarization dependence of laser damage growth was carried by Rasedujjaman *et al.* on thin oxide films [12]. They showed damage morphologies with privileged directions perpendicular to the polarization direction. They assumed that the presence of defects provides nanovoids which interact with the incident laser beam and influence the EFI distribution. Furthermore, they simulated with Finite Element Method (FEM) the impact of nanovoids on the EFI distribution and the results showed that the electric field was enhanced in the direction orthogonal to the polarization direction, in good agreement with experimental results. Similar observations and interpretations were made by Peters *et al.* with a UV laser in the nanosecond regime with polarization dependence in coatings attributed to asymmetrical E-field intensification on defects [13].

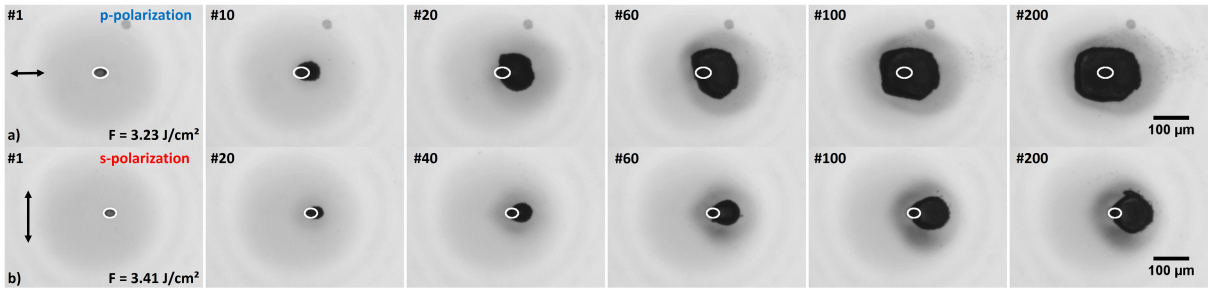

Fig. 1. Acquisitions of damage growth sequences with the microscope. Initial damage sites were illuminated (a) in *p*-polarization at a fluence of 3.23 J/cm^2 and (b) in *s*-polarization at a fluence of 3.41 J/cm^2. The laser beam comes from the left with an angle of incidence of 45°. The white ellipses represent contours of the initial damage sites. The black arrows represent the polarization direction. See Visualization 1 for complete sequences.

Here, we investigate the influence of the polarization on high-reflective MLD mirrors. Initial damage sites were illuminated with a spatially top-hat beam in *s* and *p*-polarization. We determine Laser-Induced Damage Growth Threshold (LIDGT) and we measure damage growth dynamics through growth coefficients. A numerical model based on FEM has been developed to improve the understanding by reproducing damage growth sequences.

Experiments were carried out on MLD mirrors optimized to operate in ambient air and to provide a reflectivity higher than 99%, in *s*- and *p*-polarization at 1053 nm with an angle of incidence of 45°. The mirror design is [Fused silica / (HL)^{17} H xL yH / Air], where H and L represent Quarter Wave Optical Thickness (QWOT) layers of HfO_2 and SiO_2 respectively. x and y are coefficients set to reduce the EFI peak within the outer layer by using optimization algorithm presented in Ref. [14]. Laser damage tests were performed under ambient air at 800 fs and 45° of incidence on the laser damage setup presented in Ref. [15]. The laser source (Amplitude Système, S pulse HP) provides a spatially Gaussian beam centered at 1053 nm. Damage initiation thresholds were measured at (6.12 ± 0.11) J/cm^2 for *s*-polarized beam and (3.83 ± 0.18) J/cm^2 for *p*-polarized beam.

Damage growth study was performed in ambient air on the same laser damage set-up using the same laser source. A pair of fused silica phase plate (FBS2, Ekspla) and a 30 cm focal lens are used to transform the circular Gaussian beam into a square top-hat beam with 150 μm at Full Width at Half Maximum (FWHM), described in Ref.[16, 17]. The top-hat beam profile is equivalent to super-Gaussian profile of order 6. The use of the top-hat beam aims at avoiding the intensity gradient of Gaussian beams to facilitate the interpretation of results [16]. First, identical damage sites were initiated with a Gaussian beam at a fluence 10% above the LIDT in *p*-polarization. The influence of the initial damage site was studied. For that purpose, we initiated and illuminated initial damage sites in both *s*- an *p*-polarizations. We observed small damage growth rate discrepancies only at low fluence in *s*-polarization. Then, these damage sites were illuminated with the top-hat beam at different fluences for both polarizations at an angle of incidence of 45° and 0.8 ps of pulse duration. For each fluence, three different sites were illuminated under the same conditions to validate the repeatability of the measurement. An *in-situ* visualization system composed of a microscope and a camera was implemented to image the surface of the sample.

Figure.1 shows different image sequences using the microscope of damage growth experiments according to the two polarizations at similar fluences. Figure 1(b) shows an asymmetry of the final damage site morphology in *s*-polarization at low fluence compared to the LIDT$_s$. For higher fluences, we obtained a final damage site in *s*-polarization similar to that observed in *p*-polarization (Fig.1(a)#200). From these images, the damaged area is measured by image processing. The evolution of the damaged area is characterized by a linear relation $S_N = \beta \times N + S_0$ [11, 16, 18]. The initial area and the damaged area after N shots are defined by S_0 and S_N (μm^2) respectively, the linear growth coefficient is represented by β (μm^2/shot). The damage growth coefficient β for a given fluence is the average value of the three measured growth coefficients.

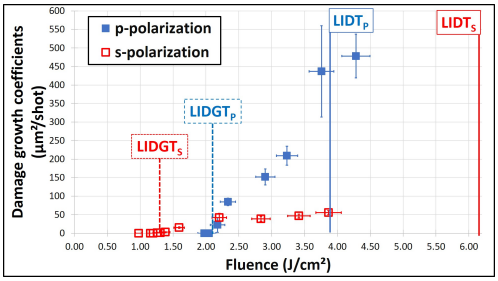

Fig. 2. Evolution of the damage growth coefficients as a function of the fluence according to the polarization.Vertical error bars represent the standard deviation between the 3 measured growth coefficients.

Figure.2 shows the evolution of the damage growth coefficients as a function of the fluence according to the polarization. The vertical error bars correspond to the standard deviations between the three measured coefficients which demonstrate a good repeatability. First, one can see that the LIDGT has distinct values depending on the polarization, designated as LIDGT$_s$ for *s*-polarization and LIDGT$_p$ for *p*-polarization. The LIDGT is defined as the average value between the last fluence with growth coefficient equals to zero and the first fluence with a non-zero growth coefficient. Indeed, the LIDGT$_s$ and the LIDGT$_p$ were measured at 1.23 ± 0.04 J/cm^2 and 2.11 ± 0.09 J/cm^2 respectively which corresponds to approximately 20% and 55% of the LIDT$_s$ and the LIDT$_p$ respectively. We assumed that the difference between our results and those reported in Ref. [11] comes from the sample designs and the manufacture process. Second, even though LIDGT$_s$ has a lower value than LIDGT$_p$, the damage growth dynamics is slower in s-polarization than in p-polarization, as shown in Fig.2. Third, different damage

site morphologies according to the polarization are observed. Damage growth experiments were repeated on a different MLD mirror design with similar results, which highlights the reproducibility of the influence of the polarization. SEM images with a better resolution were captured on this second mirror to highlight the two damage site morphologies displayed in Fig.3. Rasedujjaman *et al.* and Obara *et al.* found similar features during damage growth sequences on thin oxide films and SiC crystals [12, 19]. They demonstrated numerically that the EFI distribution is enhanced in a direction orthogonal to the polarization as observed experimentally.

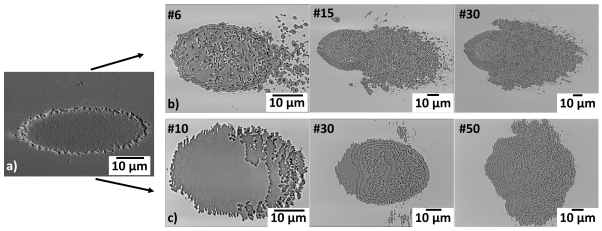

Fig. 3. SEM images of (a) an initial damage site and damage morphologies at different steps of the growth in (b) *s*-polarization and (c) *p*-polarization. The fluence corresponds to 70% of the respective LIDT, which represents a fluence of 1.80 J/cm^2 and 2.57 J/cm^2 in *p*- and *s*-polarization respectively.

A numerical 2D model based on the FEM to simulate damage growth sequence was developed in Ref. [17]. The main goal of this model is to assess the trends observed experimentally. It was assumed that the EFI distribution evolves with the new damaged structure for each laser shot. The model was developed to calculate the evolution of the EFI distribution and to simulate damage process. However, the interpretation was limited by the representation of the mirror design in one plane (2D simulations), which limits the study of polarization effects. A 3D model is required to study the impact of the polarization on the damage growth. The geometry represents the mirror design used during the experiments (see Fig.4(a)) with a size limited to $7\times7\times9$ μm^3 due to computational resources. An elliptical cylinder of 3 and 2 μm of major and minor axis respectively was added to the top layer of the mirror to represent the initial damage site (see Fig.1(a)). A linearly polarized plane wave is propagated from the air for an incidence of 45°. The EFI distribution induced by the damage site is calculated in two steps. First, the model solves the Maxwell's equations with the FEM for the pristine mirror (without damage sites) and provides a background field. Then, the background field is set as a source term to calculate the EFI distribution with the scattered field method for the damaged structure (see Fig.4(b)). At this stage, nodes where the intrinsic LIDT is reached (see Fig.4(c)) have their refractive index set to 1 (refractive index of air) to simulate the occurrence of damage sites in the volume of the multilayer (see Fig.4(d)). These 3 steps represent one iteration. The next iteration will use the new damaged structure as a starting point for the calculation of the EFI. Damage growth sequences at different fluences were calculated by considering 5 iterations for *s*-polarization and 10 iterations for *p*-polarization (see Visualization 2). The damage area was measured on the top layer to compare with experimental measurements. The evolution was also characterized by an affine relationship to determine damage growth coefficients, shown in Fig.5. The model highlights similar trends to those observed experimentally with the $LDGT_s$ lower than the $LIDGT_p$. The

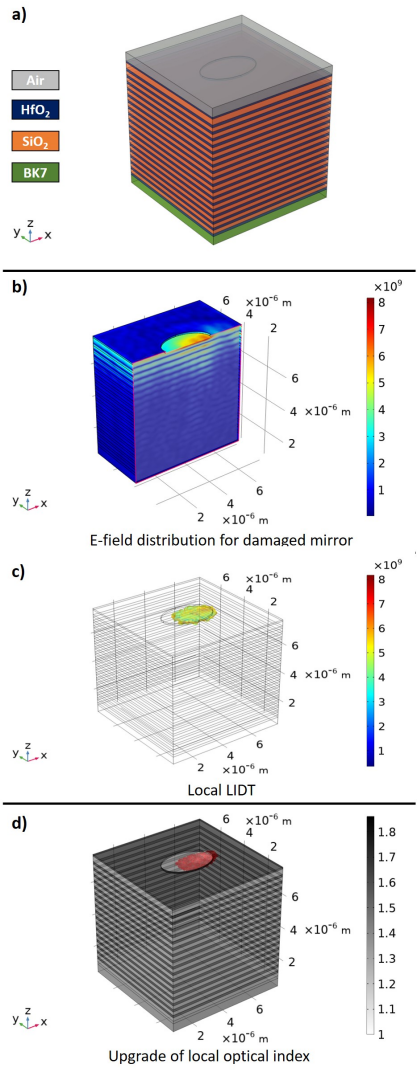

Fig. 4. (a) Representation of the geometry implemented in the FEM model which represents the MLD design used for the experiments. Description of one iteration of the FEM model. The color scale represents the EFI and the gray scale represents the refractive index. The EFI distribution is first calculated for a perfect mirror. (b) Then, the previous result is used as a source term to calculate the EFI distribution for the damaged mirror. (c) Nodes where the intrinsic LIDT is found. (d) Assigned refractive indexes with the new damaged structure. Red marks represent damaged nodes (refractive index is equal to 1).

numerical values are different from the experimental results, the model cannot reproduce the growth rate. This could be due to the size of the initial damage site and the dimension of the geometry which are not representative of the experiments. The model confirms the experimental observations with a privileged direction orthogonal to the polarization, as illustrated in Fig.6. The EFI is enhanced on a specific direction which leads to different damage site morphologies. These results support the assumption that the damage growth phenomenon is mainly driven by the electric field distribution.

To conclude, damage growth experiments were carried out in *s* and *p*-polarization on MLD mirrors with a spatially top-hat beam in the sub-picosecond regime. The evolution of the dam-

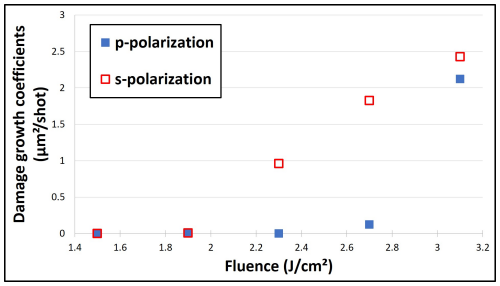

Fig. 5. Evolution of the numerical damage growth coefficients as a function of the fluence of the incident wave.

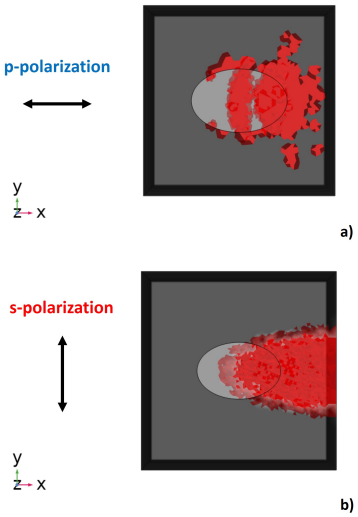

Fig. 6. Damage site morphologies after 5 iterations simulated with the FEM model according to (a) the *p*-polarization and (b) *s*-polarization. The beam comes from the left with 45° of incidence at a fluence of 3.1 J/cm^2. The red marks correspond to the damaged zone. The black arrows represent the polarization direction. See Visualization 2 for complete sequences.

aged area was described by a linear relation to deduce damage growth coefficients. Damage growth experiments were performed on several samples. On average, the values correspond to a range between 15% and 30% of the LIDT in *s*-polarization and between 50% and 60% of the LIDT in *p*-polarization. Lower damage growth dynamics were evidenced in *s*-polarization and two damage site morphologies were observed. A 3D model was developed in order to study the impact of the polarization and to assess experimental observations. The numerical model revealed similar trends to those observed experimentally and consolidates the previous assumption. All these results evidenced the fact that the EFI distribution drives the laser damage growth.

These results should motivate to improve the model, in particular the improvement of the computational resources to take into account the full size of the initial damage site. It will be interesting to include different phenomena such as the fatigue phenomenon or the deposition of residual materials (debris) during the growth [20, 21]. These phenomena could have an impact on damage growth dynamics. This model could be either adapted to different designs and be used to study damage growth on other critical components, such as gratings. The results presented in this paper involve multilayer dielectric mirrors optimized to operate in air and it will be interesting to investigate in further studies the impact of air/vacuum conditions on damage growth properties.

Disclosures. The authors declare no conflicts of interest.

Data availability. Data underlying the results presented in this paper are not publicly available at this time but may be obtained from the authors upon reasonable request.

REFERENCES

1. D. Ristau, ed., *Laser-Induced Damage in Optical Materials* (CRC Press Taylor & Francis Group, 2014).
2. M. Chorel, S. Papernov, A. A. Kozlov, B. N. Hoffman, J. B. Oliver, S. G. Demos, T. Lanternier, E. Lavastre, L. Lamaignère, N. Roquin, B. Bousquet, N. Bonod, and J. Néauport, Opt. Express **27**, 16922 (2019).
3. L. Gallais, "Laser damage resistance of optical coatings in the sub-ps regime: limitations and improvement of damage threshold," in *Laser Sources and Applications III,* , vol. 9893 J. I. Mackenzie, H. JelÍnková, T. Taira, and M. A. Ahmed, eds., International Society for Optics and Photonics (SPIE, 2016), pp. 15 – 25.
4. G. Abromavicius, R. Buzelis, R. Drazdys, A. Melninkaitis, and V. Sirutkaitis, Laser-Induced Damage Opt. Mater. (SPIE 2007) **6720**, 329 (2007).
5. H. Becker, D. Tonova, M. Sundermann, L. Jensen, M. Gyamfi, D. Ristau, and M. Mende, Opt. Syst. Des. 2015: Adv. Opt. Thin Films V **9627**, 215 (2015).
6. N. Blanchot, G. Behar, T. Berthier, E. Bignon, F. Boubault, C. Chappuis, H. Coïc, C. Damiens-Dupont, J. Ebrardt, Y. Gautheron, P. Gibert, O. Hartmann, E. Hugonnot, F. Laborde, D. Lebeaux, J. Luce, S. Montant, S. Noailles, J. Néauport, D. Raffestin, B. Remy, A. Roques, F. Sautarel, M. Sautet, C. Sauteret, and C. Rouyer, Plasma Phys. Control. Fusion **50**, 124045 (2008).
7. A. Hervy, L. Gallais, D. Mouricaud, G. Chériaux, O. Utéza, R. Clady, M. Sentis, and A. Fréneaux, Laser-Induced Damage Opt. Mater. (SPIE 2014) **9237**, 59 (2014).
8. A. A. Kozlov, J. C. Lambropoulos, J. B. Oliver, B. N. Hofman, and S. Demos, Sci. Reports **9**, 607 (2019).
9. M. Sozet, J. Neauport, E. Lavastre, N. Roquin, L. Gallais, and L. Lamaignère, Opt. Lett. **41**, 2342 (2016).
10. Y. Hao, M. Sun, Z. Jiao, Y. Guo, X. Pan, X. Pang, and J. Zhu, Appl. Opt. **57**, 4191 (2018).
11. M. Sozet, S. Bouillet, J. Berthelot, J. Neauport, L. Lamaignère, and L. Gallais, Opt. Express **25**, 25767 (2017).
12. M. Rasedujjaman and L. Gallais, Opt. Express **26**, 24444 (2018).
13. V. N. Peters, S. R. Qiu, C. Harthcock, R. A. Negres, G. Guss, T. Voisin, E. Feigenbaum, C. J. Stolz, D. Vipin, and M. Huang, J. Appl. Phys. **130**, 043103 (2021).
14. M. Chorel, T. Lanternier, Éric Lavastre, N. Bonod, B. Bousquet, and J. Néauport, Opt. Express **26**, 11764 (2018).
15. A. Ollé, J. Luce, N. Roquin, C. Rouyer, M. Sozet, L. Gallais, and Lamaignère, Rev. Sci. Instruments **90**, 073001 (2019).
16. A. Ollé, S. Diop, N. Roquin, L. Gallais, and L. Lamaignère, Opt. Lett. **45**, 4024 (2020).
17. S. Diop, A. Ollé, N. Roquin, M. Chorel, Éric Lavastre, L. Gallais, N. Bonod, and L. Lamaignère, Opt. Express **30**, 17739 (2022).
18. Y. Hao, M. Sun, Y. Guo, S. Shi, X. Pan, X. Pang, and J. Zhu, Opt. Express **26**, 8791 (2018).
19. G. Obara, H. Shimizu, T. Enami, E. Mazur, M. Terakawa, and M. Obara, Opt. Express **21**, 26323 (2013).
20. A. Rosenfeld, M. Lorenz, R. Stoian, and D. Ashkenasi, Appl. Phys. A **69**, S373 (1999).
21. K. R. P. Kafka, B. N. Hoffman, H. Huang, and S. G. Demos, Opt. Eng. **60**, 1 (2020).

FULL REFERENCES

1. D. Ristau, ed., *Laser-Induced Damage in Optical Materials* (CRC Press Taylor & Francis Group, 2014).
2. M. Chorel, S. Papernov, A. A. Kozlov, B. N. Hoffman, J. B. Oliver, S. G. Demos, T. Lanternier, E. Lavastre, L. Lamaignère, N. Roquin, B. Bousquet, N. Bonod, and J. Néauport, "Influence of absorption-edge properties on subpicosecond intrinsic laser-damage threshold at 1053 nm in hafnia and silica monolayers," Opt. Express **27**, 16922–16934 (2019).
3. L. Gallais, "Laser damage resistance of optical coatings in the sub-ps regime: limitations and improvement of damage threshold," in *Laser Sources and Applications III,* vol. 9893 J. I. Mackenzie, H. JelÍnková, T. Taira, and M. A. Ahmed, eds., International Society for Optics and Photonics (SPIE, 2016), pp. 15 – 25.
4. G. Abromavicius, R. Buzelis, R. Drazdys, A. Melninkaitis, and V. Sirutkaitis, "Influence of electric field distribution on laser-induced damage threshold and morphology of high-reflectance optical coatings," Laser-Induced Damage Opt. Mater. (SPIE 2007) **6720**, 329 – 336 (2007).
5. H. Becker, D. Tonova, M. Sundermann, L. Jensen, M. Gyamfi, D. Ristau, and M. Mende, "Advanced femtosecond laser coatings raise damage thresholds," Opt. Syst. Des. 2015: Adv. Opt. Thin Films V **9627**, 215 – 220 (2015).
6. N. Blanchot, G. Behar, T. Berthier, E. Bignon, F. Boubault, C. Chappuis, H. Coïc, C. Damiens-Dupont, J. Ebrardt, Y. Gautheron, P. Gibert, O. Hartmann, E. Hugonnot, F. Laborde, D. Lebeaux, J. Luce, S. Montant, S. Noailles, J. Néauport, D. Raffestin, B. Remy, A. Roques, F. Sautarel, M. Sautet, C. Sauteret, and C. Rouyer, "Overview of PETAL, the multi-petawatt project on the LIL facility," Plasma Phys. Control. Fusion **50**, 124045 (2008).
7. A. Hervy, L. Gallais, D. Mouricaud, G. Chériaux, O. Utéza, R. Clady, M. Sentis, and A. Fréneaux, "Thin films characterizations to design high-reflective coatings for ultrafast high power laser systems," Laser-Induced Damage Opt. Mater. (SPIE 2014) **9237**, 59 – 65 (2014).
8. A. A. Kozlov, J. C. Lambropoulos, J. B. Oliver, B. N. Hofman, and S. Demos, "Mechanisms of picosecond laser induced damage in common multilayer dielectric coatings," Sci. Reports **9**, 607 (2019).
9. M. Sozet, J. Neauport, E. Lavastre, N. Roquin, L. Gallais, and L. Lamaignère, "Laser damage growth with picosecond pulses," Opt. Lett. **41**, 2342–2345 (2016).
10. Y. Hao, M. Sun, Z. Jiao, Y. Guo, X. Pan, X. Pang, and J. Zhu, "Determination of the damage growth threshold of multilayer dielectric gratings by picosecond laser pulses based on saturation damage size analysis," Appl. Opt. **57**, 4191–4201 (2018).
11. M. Sozet, S. Bouillet, J. Berthelot, J. Neauport, L. Lamaignère, and L. Gallais, "Sub-picosecond laser damage growth on high reflective coatings for high power applications," Opt. Express **25**, 25767 (2017).
12. M. Rasedujjaman and L. Gallais, "Polarization dependent laser damage growth of optical coatings at sub-picosecond regime," Opt. Express **26**, 24444–24460 (2018).
13. V. N. Peters, S. R. Qiu, C. Harthcock, R. A. Negres, G. Guss, T. Voisin, E. Feigenbaum, C. J. Stolz, D. Vipin, and M. Huang, "Investigation of uv, ns-laser damage resistance of hafnia films produced by electron beam evaporation and ion beam sputtering deposition methods," J. Appl. Phys. **130**, 043103 (2021).
14. M. Chorel, T. Lanternier, Éric Lavastre, N. Bonod, B. Bousquet, and J. Néauport, "Robust optimization of the laser induced damage threshold of dielectric mirrors for high power lasers," Opt. Express **26**, 11764–11774 (2018).
15. A. Ollé, J. Luce, N. Roquin, C. Rouyer, M. Sozet, L. Gallais, and Lamaignère, "Implications of laser beam metrology on laser damage temporal scaling law for dielectric materials in the picosecond regime," Rev. Sci. Instruments **90**, 073001 (2019).
16. A. Ollé, S. Diop, N. Roquin, L. Gallais, and L. Lamaignère, "Temporal dependency in the picosecond regime of laser damage growth," Opt. Lett. **45**, 4024–4027 (2020).
17. S. Diop, A. Ollé, N. Roquin, M. Chorel, Éric Lavastre, L. Gallais, N. Bonod, and L. Lamaignère, "Investigation of the influence of a spatial beam profile on laser damage growth dynamics in multilayer dielectric mirrors in the near infrared sub-picosecond regime," Opt. Express **30**, 17739–17753 (2022).
18. Y. Hao, M. Sun, Y. Guo, S. Shi, X. Pan, X. Pang, and J. Zhu, "Asymmetrical damage growth of multilayer dielectric gratings induced by picosecond laser pulses," Opt. Express **26**, 8791–8804 (2018).
19. G. Obara, H. Shimizu, T. Enami, E. Mazur, M. Terakawa, and M. Obara, "Growth of high spatial frequency periodic ripple structures on sic crystal surfaces irradiated with successive femtosecond laser pulses," Opt. Express **21**, 26323–26334 (2013).
20. A. Rosenfeld, M. Lorenz, R. Stoian, and D. Ashkenasi, "Ultrashort-laser-pulse damage threshold of transparent materials and the role of incubation," Appl. Phys. A **69**, S373–S376 (1999).
21. K. R. P. Kafka, B. N. Hoffman, H. Huang, and S. G. Demos, "Mechanisms of picosecond laser-induced damage from interaction with model contamination particles on a high reflector," Opt. Eng. **60**, 1 – 20 (2020).